Journal of Colloid and Interface Science 478 (2016) 246–255

Contents lists available at ScienceDirect

Journal of Colloid and Interface Science

journal homepage: www.elsevier.com/locate/jcis

Controllable degradation of medical magnesium by electrodeposited composite films of mussel adhesive protein (*Mefp-1*) and chitosan

Ping-Li Jiang [a], Rui-Qing Hou [a], Cheng-Dong Chen [a], Lan Sun [a,*], Shi-Gang Dong [b], Jin-Shan Pan [c], Chang-Jian Lin [a,b,*]

[a] State Key Laboratory for Physical Chemistry of Solid Surfaces, and College of Chemistry and Chemical Engineering, Xiamen University, Xiamen 361005, China
[b] College of Energy and School of Energy Research, Xiamen University, Xiamen 361005, China
[c] Div. of Surface and Corrosion Science, Dept. of Chemistry, Royal Institute of Technology, Drottning Kristinasväg, 51, SE-100 44 Stockholm, Sweden

GRAPHICAL ABSTRACT

A composite film of chitosan/*Mefp-1*/chitosan was electrodeposited on Mg surface, which exhibited continually increased corrosion resistance, controlled the degradation rate of Mg and elevated the biocompatibility of the substrate greatly.

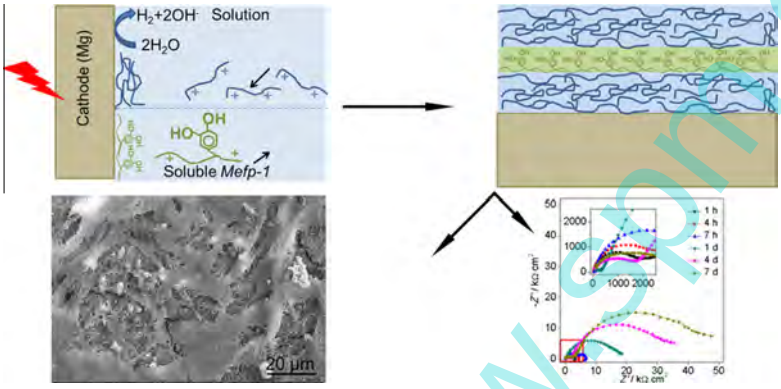

ARTICLE INFO

Article history:
Received 3 April 2016
Revised 29 May 2016
Accepted 1 June 2016
Available online 2 June 2016

Keywords:
Mussel adhesive protein (*Mefp-1*)
Chitosan
Magnesium
Corrosion protection
Biocompatiblity

ABSTRACT

To control the degradation rate of medical magnesium in body fluid environment, biocompatible films composed of Mussel Adhesive Protein (*Mefp-1*) and chitosan were electrodeposited on magnesium surface in cathodic constant current mode. The compositions and structures of the films were characterized by atomic force microscope (AFM), scanning electron microscope (SEM) and infrared reflection absorption spectroscopy (IRAS). And the corrosion protection performance was investigated using electrochemical measurements and immersion tests in simulated body fluid (Hanks' solution). The results revealed that *Mefp-1* and chitosan successfully adhered on the magnesium surface and formed a protective film. Compared with either single *Mefp-1* or single chitosan film, the composite film of chitosan/*Mefp-1*/chitosan (CPC (chitosan/*Mefp-1*/chitosan)) exhibited lower corrosion current density, higher polarization resistance and more homogenous corrosion morphology and thus was able to effectively control the degradation rate of magnesium in simulated body environment. In addition, the active attachment and

* Corresponding authors at: State Key Laboratory for Physical Chemistry of Solid Surfaces, and College of Chemistry and Chemical Engineering, Xiamen University, Xiamen 361005, China (C.-J. Lin).
E-mail addresses: sunlan@xmu.edu.cn (L. Sun), cjlin@xmu.edu.cn (C.-J. Lin).

http://dx.doi.org/10.1016/j.jcis.2016.06.001

spreading of MC3T3-E1 cells on the CPC film coated magnesium indicated that the CPC film was significantly able to improve the biocompatibility of the medical magnesium.

1. Introduction

As the most promising biodegradable metallic biomaterials, magnesium and its alloys have drawn considerable attention due to their excellent biocompatible and mechanical properties. In particular, the elastic modulus and density of Mg and its alloys are similar to those of the natural bone of human. Magnesium can be bio-adsorbed through electrochemical corrosion in human body environment, which may avoid a second surgery for implant removal. Mg^{2+}, the degradation product, is beneficial to bone growth and strength, and meanwhile, excessive Mg^{2+} can be naturally excluded out of human body with the urine [1–5]. However, too rapid degradation rate and excessive hydrogen bubbles generated from the corrosion process in body environment still largely hinder clinical applications of biomedical Mg and Mg alloys [6].

To realize a controllable biodegradation of medical Mg-based alloys for clinical applications, various strategies have been developed, including alloying design, processing, heat treatment, surface modification, etc. [7–9]. Among these methods, the protective film is an effective approach to improve the biodegradation behavior of Mg alloys [10]. It is needed to develop a protective film for not only the controllable degradation of medical Mg-based materials to fit the recovery of bone tissue, but also the sufficient biocompatibility and bio-safety in human body environment. Mussel Adhesive Proteins (MAPs) and chitosan have been respectively proved to be fully 'green' bio-products in clinical application due to their excellent adhesion and biocompatibility [11–13] as well as protective properties [14–16].

MAPs are extracted from mussel byssus and have been identified as six proteins which are respectively named as *Mytilus Edulis* foot protein-1 (*Mefp-1*) to protein-6 (*Mefp-6*) [17]. Among them, *Mefp-1*, the first adhesive protein, is the key component on the outer cuticle of byssal threads [18], and has a high isoelectric point (pI = ~10.3), large molecular weight (~108 kDa) [19] and automatic film-forming property. Di-hydroxyphenylalanine (DOPA), a chief residue of *Mefp-1* [20], is primarily responsible for the excellent cohesive properties via hydrogen bonding [21], cross-linking [22] and covalent bonding [23]. As shown in Fig. 1a [12], the structure of *Mefp-1* has repetitive decapeptide unit. It has been reported that *Mefp-1* has excellent corrosion protective, biocompatible and adhesive properties, and it can be used as a fully green inhibitor to protect carbon steel against corrosion [15,24,25] and also used as a biomedical adhesive in clinical application [26].

Chitosan [13,27], the partially deacetylated products of chitin, is an abundant natural amino polysaccharid extracted from the exoskeletons of insects and marine invertebrates. Fig. 1b and 1c show the structure of chitosan and cellulose, respectively. Clearly, the structure of chitosan and cellulose is similar, which is favorable to the high biological activity of chitosan [28]. Chitosan contains various functional groups, such as amine, hydroxyl and pyranoid

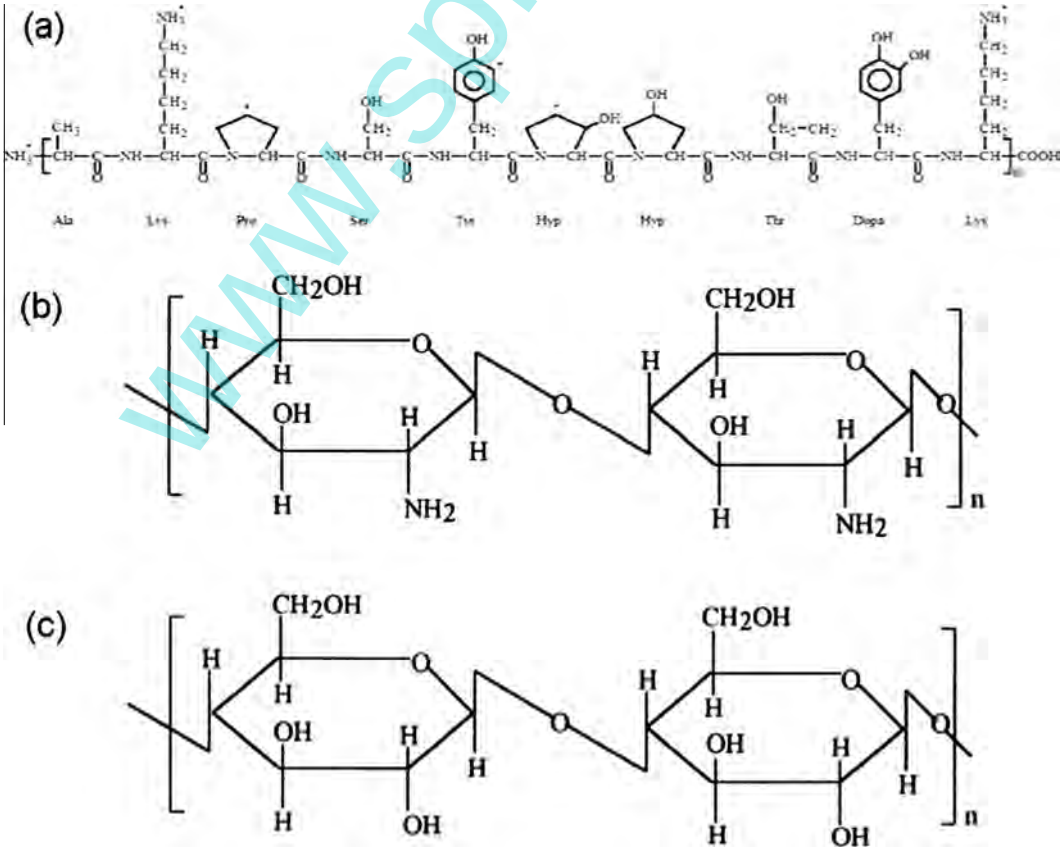

Fig. 1. The chemical structure of (a) *Mefp-1* [12], (b) chitosan and (c) cellulose [28].

ring, etc., which initiate the biodegradation, quaternization and chelation [13]. Due to the good adhesive property, superior film-forming ability, outstanding biological activity and reversible complexation property [29], chitosan has been widely used in cosmetics, drug delivery, biomedicine [13] and corrosion protection [30,31].

This study aims to develop a biocompatible and protective film on magnesium surface for its controllable degradation in physiologic conditions for biomedical applications. The films composed of *Mefp-1* or/and chitosan were prepared by electrodeposition and characterized by SEM, AFM and IRAS. The degradation behaviors and biocompatibility of the as-prepared films coated on magnesium were evaluated by electrochemical measurements, immersion tests and *in vitro* cell cultures.

2. Materials and methods

2.1. Materials and solutions

Pure Mg (99.99 wt%) discs of Φ 11 mm × 8 mm cut from a rod were used in this study. The samples for immersion tests and electrochemical impedance spectroscopy (EIS) measurements were imbedded in epoxy resin with one circular face exposed as working surface. The Mg specimens were abraded successively with SiC papers from 400 # to 1500 #, then polished respectively with 1.0 and 0.3 μm Al_2O_3 powders, and finally ultrasonically cleaned in ethanol for 10 min before experiments.

The chitosan (D.D 75–85%) with medium molecule weight (190,000–310,000 based on viscosity) purchased from Sigma-Aldrich was dissolved by aqueous acetic acid (1 vol%) and then stirred for 24 h to obtain 1 mg mL^{-1} chitosan solution. The residue was filtered out and the pH value of the solution was adjusted to 4.6 with NaOH solution before use. The mussel adhesive protein (*Mefp-1*) dissolved in 1 wt% citric acid was supplied by Biopolymer Products AB (Gothenburg, Sweden) and saved in the dark at 4 °C. The *Mefp-1* solution was diluted using 1 wt% citric acid with pH 4.6 to a concentration of 1 mg mL^{-1}. The Hanks' solution used as test solution was comprised of 8.0 g L^{-1} NaCl, 0.4 g L^{-1} KCl, 0.14 g L^{-1} $CaCl_2$, 0.35 g L^{-1} $NaHCO_3$, 0.35 g L^{-1} D-$C_6H_5O_6$, 0.2 g L^{-1} $MgSO_4{\cdot}7H_2O$, 0.1 g L^{-1} KH_2PO_4 and 0.06 g L^{-1} $Na_2HPO_4{\cdot}12H_2O$ and its pH value was adjusted to 7.2–7.4 using tris(hydroxymethyl)aminomethane and HCl solutions [32]. The temperature was kept at 37 ± 1 °C during the tests using a water bath. All of the reagents were analytically pure.

2.2. Film preparation

The *Mefp-1* film and chitosan film on Mg substrate were prepared through electrodeposition respectively in the 1 mg mL^{-1} *Mefp-1* solution and the 1 mg mL^{-1} chitosan solution at −1.0 mA cm^{-2} for 10 min. The CPC film was prepared by electrodepositon in chitosan, *Mefp-1* and chitosan solutions in turn at the same conditions. In the electrodeposition process in acidic solutions, *Mefp-1* and chitosan molecules with positive charges moved towards the cathode under the electric field and formed insoluble film on Mg substrates due to the high pH generated by the cathodic hydrogen evolution reaction [33]. Subsequently, the samples were dried in an oven at 60 °C for 20 min after each electrodeposition to densify the film by evaporating the residual acidic solvent and water in the coating, and to increase the water resistance of the films by accelerating the cross-linking of *Mefp-1* or chitosan molecules [34–37].

2.3. Characterization of SEM and AFM

The morphologies of the as-prepared films were characterized by the field emission gun scanning electron microscope (Zeiss Sigma SEM, Carl Zeiss Co., Ltd., Germany) equipped with energy dispersive X-ray analyzer (EDX) using an acceleration voltage of 15 kV. Samples for the cross-sectional characterization were prepared by mounting the Mg coated with different films in a mode of epoxy resin, and then cutting the sample to expose the side face. Before observation with SEM, the samples were mechanically ground with SiC abrasive paper, polished with Al_2O_3 powders and finally sputter coated with a thin platinum film. The surface characteristics and roughness of the films were evaluated using the CSPM-5500 atomic force microscope (AFM) with silicon tip probe of a spring constant of 40 N m^{-1} and a resonant frequency of 300 kHz at the tapping mode with a sweep speed of 1 Hz. The obtained images were analyzed by CSPM Imager Analysis. The roughness was identified with the surface roughness parameter R_a and R_q, which are the arithmetic average and standard deviation of the surface height values respectively [24]. R_a and R_q were calculate as follows:

$$R_a = \frac{1}{N}\sum_{j=1}^{N}|Z_j| \tag{1}$$

$$Rq = \sqrt{\frac{\sum_{j=1}^{N}(Z_j)^2}{N}} \tag{2}$$

where Z_j represents the local Z value and N is the number of points.

2.4. IRAS analysis

Infrared reflection absorption spectroscopy (IRAS) analysis was performed by a Nicolet-8700 FT-IR equipped with a MCT-B detector. The spectra were obtained at a resolution of 4 cm^{-1} in the wavenumber range of 400–4000 cm^{-1} using 1024 scans.

2.5. Immersion tests

Immersion degradation tests of bare Mg and Mg coated with the *Mefp-1* film, the chitosan film and the CPC composite film were performed in Hanks' solution. After immersion for 7 d, the surface compositions and morphologies of the specimens were characterized by IRAS and SEM, respectively.

2.6. Electrochemical measurements

The corrosion protection properties of the coated Mg with various films in Hanks' solution were evaluated by EIS and potentiodynamic polarization [33]. All electrochemical measurements were carried out using AutoLab PGSTAT302N work station (ECO Chemie B.V., Netherlands) with a typical three-electrode cell, in which the coated Mg samples were used as working electrode, saturated calomel electrode (SCE) as the reference electrode and a platinum electrode as the counter electrode.

The EIS measurements were carried out in Hanks' solution at an open circuit potential with the frequency range of 10^5–10^{-2} Hz and AC voltage amplitude of 10 mV. The spectra were measured after immersion for 1 h, 4 h, 7 h, 1 d, 4 d and 7 d.

The potentiodynamic polarization measurements were performed after 7 d of immersion in Hanks' solution from −0.25 to 1.0 V vs. OCP at a scan rate of 1 mV s^{-1}. The corrosion current density (i_{corr}) was analyzed by General Purpose Electrochemical System (GPES) equipped with Corrosion Rate Procedure according to the following equation [15,38]:

$$I = i_{corr}\left\{\exp\left(\frac{2.3\Delta E}{b_c}\right) - \exp\left(\frac{2.3\Delta E}{b_a}\right)\right\} \tag{3}$$

All electrochemical tests were repeated for at least three times for statistical purpose.

2.7. Cell culture

In order to identify the biocompatibility of the CPC film coated Mg, mouse osteoblast-like cells MC3T3-E1 were used in the culture evaluation. Mg and the CPC film coated Mg discs were sterilized in an autoclave before cell seeding. DMEM/F12 containing 10% fetal bovine serum (FBS) medium was supplied for culturing cells on specimens (5×10^4 cells cm^{-3} in density) in an incubator at 37 °C with 5% CO_2 for 4 d. For the cell morphology observation, the unattached cells and the culture medium were removed, followed by washing the specimens three times with phosphate-buffered saline (PBS, pH 7.4). Then, the cells were fixed by 2.5% glutaraldehyde solution, rinsed with PBS and dehydrated in 30 vol%, 50 vol%, 75 vol%, 90 vol%, and 100% (twice) ethanol solutions, successively.

3. Results and discussions

3.1. Surface morphology

Fig. 2 gives the typical AFM images of bare Mg and various films on Mg surfaces. It can be seen that the surface of the bare Mg substrate was covered by many nanoparticles, and some distinct defects and scratches which resulted from the pre-treatment process of Mg substrate can be observed (Fig. 2a). In contrast, there were no scratches on the film coated Mg samples (Fig. 2b–d), indicating the films provided a full coverage on the substrates. All of the films were composed of nanoparticles in a size range of 10–100 nm. Compared with the *Mefp-1* film, the chitosan and CPC films consisted of bigger nanoparticles from the aggregation of the smaller nanoparticles due to the viscous characteristic of chitosan solution and the polymerization of chitosan molecules during the electrodeposition.

Table 1 provides the statistic evaluation of surface roughness of bare Mg and the film coated Mg samples. It can be seen that the polished Mg surface was very smooth. The *Mefp-1* film coated sample presented a relatively lower roughness value, suggesting the *Mefp-1* film was homogenous and uniform. In contrast, the surface roughness parameters of the chitosan and CPC films were higher, which resulted from the different deacetylation degree of chitosan molecules [39] and the corrosion of Mg substrates during the film formation. Furthermore, the increase of electrodeposition times made the CPC film surface rougher, resulting from the filling and interaction between protein and chitosan.

Table 1
The statistic evaluation of surface roughness.

Roughness (nm)	Bare Mg	*Mefp-1* film	Chitosan film	CPC[a] film
R_a	2.37	10.4	14.8	19.4
R_q	3.13	13.5	19.5	23.8

[a] CPC: chitosan/*Mefp-1*/chitosan.

The SEM images of various prepared films on Mg substrate are shown in Fig. 3. Obviously, the *Mefp-1* film consisted of many nanoparticles (Fig. 3a), while the chitosan film and the CPC film exhibited glue-like topographies (Fig. 3b and 3c), but less uniform than the *Mefp-1* film, which was in accordance with the AFM results. In addition, no evident defects, pores or cracks were observed on the film surfaces, indicating that the films were intact, fully covered on the substrate and could insulate the substrate from the surrounding solution effectively compared with those porous or cracked surface coatings by alkaline treatment, anodizing treatment and fluoride treatment [40]. Some interfacial reactions such as covalent bonding, hydrogen bonding and cross-liking among the *Mefp-1* or chitosan molecules and the post heat treatment could give rise to the crackless characteristics. The average thickness of the CPC film identified by the profile images was 714.6 ± 0.05 nm, thicker than that of the chitosan film (402.0 ± 0.1 nm) and *Mefp-1* film (127.3 ± 0.8 nm). All of the three

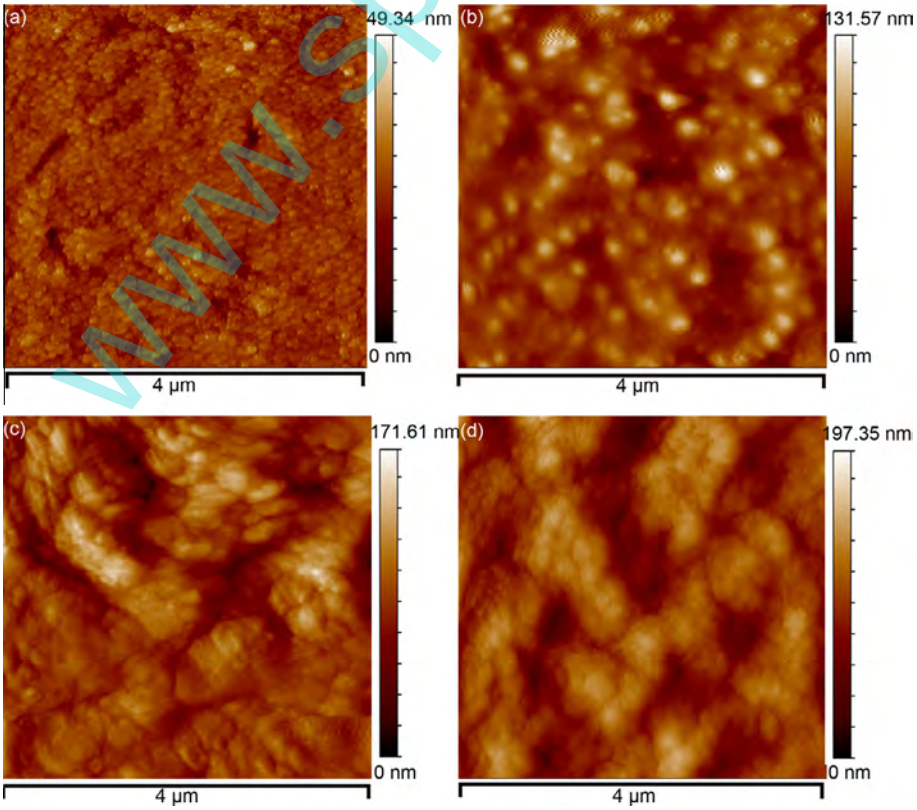

Fig. 2. AFM images of (a) pure magnesium, (b) the *Mefp-1* film, (c) the chitosan film and (d) the CPC film on Mg substrate. Scan area is 4 μm × 4 μm.

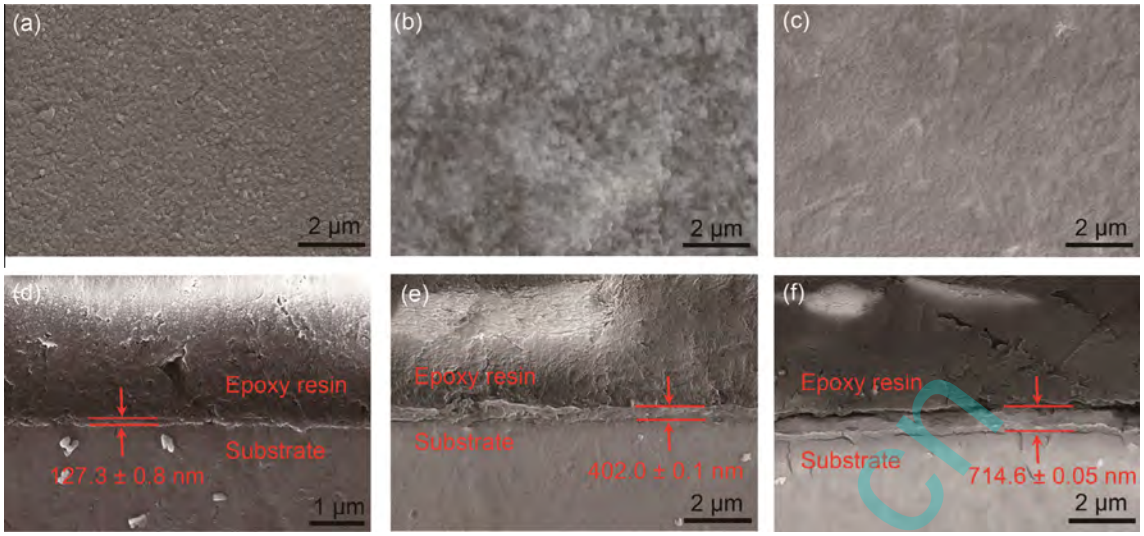

Fig. 3. SEM micrographs and profile images of (a,d) the *Mefp-1* film, (b,e) the chitosan film and (c,f) the CPC film on Mg substrate.

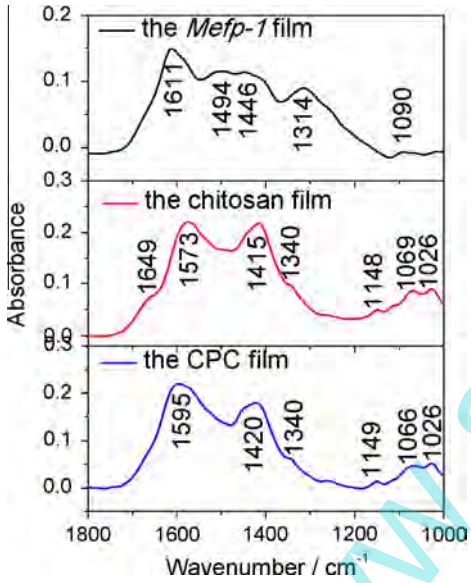

Fig. 4. IRAS spectra for the *Mefp-1* film, the chitosan film and the CPC film on Mg.

films showed a certain adhesiveness to the Mg substrate. More importantly, compared to the *Mefp-1* film and chitosan film, the CPC film displayed remarkably homogenous and entire coverage on the Mg substrate.

3.2. IRAS analysis

Fig. 4 shows the IRAS spectra in the wavenumber range of 1000–1800 cm^{-1} for different films electrodeposited on Mg. The results confirmed that the *Mefp-1* and chitosan were successfully immobilized on the Mg substrates. More specifically, the IRAS spectrum of the *Mefp-1* film presented the C=O stretching of amide in the backbone at 1611 cm^{-1}, C=C stretching of aromatic ring of DOPA side chain at 1494 cm^{-1}, N—H stretching of backbone at 1446 cm^{-1}, and C—O stretching of DOPA hydroxyl groups at 1314 cm^{-1}. The vibration of the backbone and the stretching of C—O are responsible for the band at 1090 cm^{-1} [11,24]. The characteristic absorption peaks of the chitosan film at 1649 cm^{-1} (amide I) and 1573 cm^{-1} (amide II) were the proof of the existence of chitosan on Mg surface. The deacetylation of chitosan led to the weak absorption peak of amide I at 1649 cm^{-1}. In addition, the bands at 1415 cm^{-1} and 1340 cm^{-1} were associated with the coupling of N—H angular deformation and C—N axial stretching. The stretching of C—O, C—O—C and glycosidic bonds of the polysaccharide backbone gave rise to the peaks at the range of 1000–1200 cm^{-1} [29].

It should be noted that the characteristic peaks of the CPC film was approximately the same as those of the chitosan film, which may be caused by the outmost chitosan layer of CPC film. However, a large shift for the band at 1573 cm^{-1} and the absence of the shoulder band at 1649 cm^{-1} can be observed in the IRAS spectrum of the CPC film, which may result from the overlap between the bands of chitosan and *Mefp-1* films. Another possible reason is the formation of the new C=N bond produced from the Michael's addition reaction between chitosan and the oxidation product (dopaminoquinone) of *Mefp-1* and oxgen [41], which was also able to largely improve the integrity and compactness of CPC film.

3.3. Corrosion protection properties

EIS, as a noninvasive measurement, can not only evaluate the corrosion resistance for various prepared films, but also follow the interfacial process during the degradation of Mg materials [42]. The EIS measurements of the bare Mg and Mg coated with three types of films were carried out in Hanks' solution for up to 7 d. The Nyquist plots shown in Fig. 5 displayed two or three time constants, including two capacitive loops in the initial immersion and a newly produced capacitive loop at high frequency with the prolonged immersion time which was ascribed to the generation of corrosion product film. The Nyquist plots were fitted with the equivalent circuit (a) $R_s(C_fR_f)(C_{dl}R_{ct})$ and (b) $R_s(C_{cp}R_{cp})(C_fR_f)(C_{dl}R_{ct})$ [43–45] by ZsimpWin software. Where, R_s is the resistance of the electrolyte solution between the reference electrode and working electrode. R_{ct} (the charge transfer resistance) is parallel to the double layer constant phase element (CPE), C_{dl}. R_f (the film resistance) is parallel to the CPE attributed to the film layer, C_f. The new CPE, C_{cp}, resulted from the corrosion product layer is parallel to R_{cp} (the corrosion product resistance). In general, the EIS plots vary with the interfacial process related to the surface reactivity, surface treatments and immersion time.

The fitting results of EIS for the bare Mg, the *Mefp-1* film, the chitosan film and the CPC film coated Mg immersed in Hanks' solution for different time were presented in Fig. 6. It was clear that the

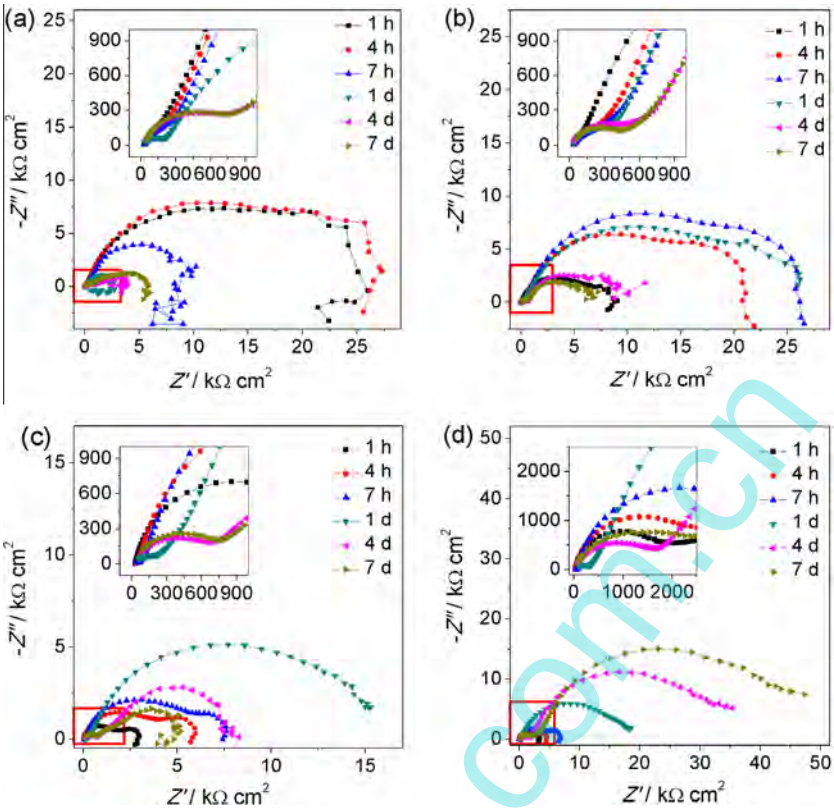

Fig. 5. Nyquist plots of (a) the bare Mg, (b) the *Mefp-1* film, (c) the chitosan film and (d) the CPC film coated Mg immersed in Hanks' solution at different time.

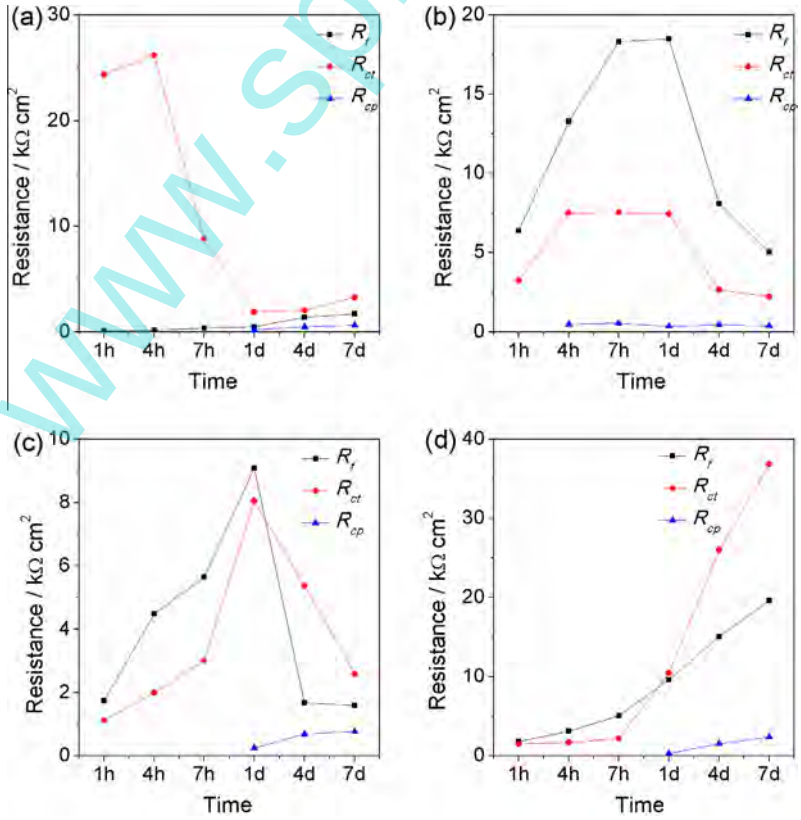

Fig. 6. Charge transfer resistance, R_{ct}, film resistance, R_f, and corrosion product resistance, R_{cp}, of (a) the bare Mg, (b) the *Mefp-1* film, (c) the chitosan film and (d) the CPC film coated Mg immersed in Hanks' solution at different time.

R_{cp} of the four samples were much lower than the R_{ct} and R_f and increased slightly with immersion time. The R_{ct} of bare Mg was much higher than the R_f in the initial time and then dropped dramatically with the increase of immersion time, while the R_f remained at a relative constant value. The high R_{ct} was due to the partial protection of oxidation film and some inhibitors in Hanks' solution such as HCO_3^- [46], and the subsequent decrease indicated that the further penetration of corrosive electrolyte and consumption of HCO_3^- led to the active dissolution of Mg substrate [43]. After 1 d of immersion, the R_{ct} and R_f increased slightly, which may be caused by the precipitation of corrosion products.

Completely different from the bare Mg, the R_{ct} of the *Mefp-1* film and the chitosan film coated Mg were lower than the R_f in the initial exposure. Both R_{ct} and R_f increased gradually with time and reached maximums at 1 d of immersion (the R_{ct} and R_f of the *Mefp-1* film coated Mg reached 7.438 kΩ cm^2 and 18.48 kΩ cm^2 respectively, and the R_{ct} and R_f of the chitosan film coated Mg were 8.048 kΩ cm^2 and 9.085 kΩ cm^2 respectively), suggesting that the *Mefp-1* film and the chitosan film may protect the Mg substrates against corrosion for a period. Nevertheless, with prolonged immersion, the scattered EIS data in low frequencies and the sharp decline of R_{ct} and R_f were measured, implying that Mg substrate suffered from localized corrosion and the films broke down or even delaminated from the Mg substrate [47]. The change tendencies of R_{ct} and R_f with immersion time demonstrated that the *Mefp-1* film and the chitosan film coated on Mg surface could only partly protect the Mg substrate from corrosion for a short period, indicating the protective abilities of these two films were too weak to offer effective protections for medical Mg alloys.

Interestingly, the R_{ct} and R_f of Mg coated with the CPC film increased constantly with immersion time, especially after 1 d of exposure. At 7 d immersion, the R_{ct} and R_f reached 36.87 kΩ cm^2 and 19.64 kΩ cm^2, respectively. Theoretically, the value of R_{ct} could be the most suitable parameter for evaluating the corrosion protection property of the films [48]. Consequently, the CPC film coated on Mg provided an effective protection, which was even continually enhanced with the immersion time. This characteristic of corrosion resistance of the CPC film is really unusual compared to the oxidation films [49], fluoride conversion coatings [50], apatite coatings [51] and polymer coatings [52] on Mg-based materials surfaces. The corrosion resistance of those previously reported films on Mg or Mg alloys was usually high at the initial tests but decreased with immersion time. The gradual increase of protection property of the CPC film for Mg may be attributed to the synergistic reaction of *Mefp-1* and chitosan which chelated with Mg^{2+} during the extended immersion time [13,53], as schematically illustrated in Fig. 7, resulting in a more compact structure and better corrosion protection property of the composite film. Further studies are needed to deeply understand the details about this phenomenon.

To further investigate the protective properties of the films, the potentiodynamic polarization curves were measured after 7 d of exposure to the Hanks' solution, as shown in Fig. 8. Comparing with the bare Mg, the corrosion potentials of Mg shifted negatively and partial passivity appeared on the anodic polarization curves when deposited with different films, demonstrating that the anodic dissolution of Mg was retarded by the films [54]. Especially, the sample coated with the CPC film exhibited the lower corrosion current density and wider passive region, indicating that the CPC film was able to provide a better protection for the Mg substrate in simulated body fluid (Hanks' solution).

The polarization curves were analyzed by the fitting software to obtain the corrosion current density, i_{corr}, corrosion potential, E_{corr}, and polarization resistance, R_p. The detail data were listed in Table 2, with an exception of bare Mg because there was no passive region for the anodic branch of bare Mg. Notably, the i_{corr} value of the CPC film coated sample was 2–8 times lower than those of the

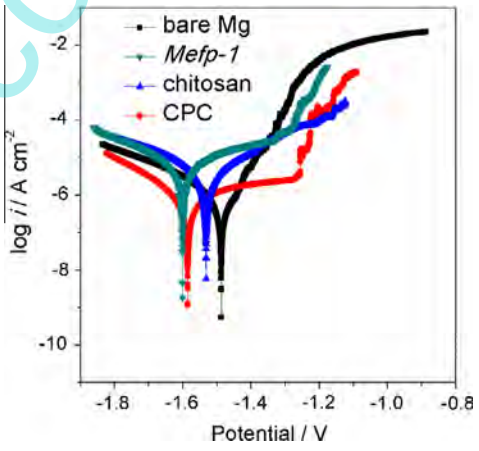

Fig. 8. Potentiodynamic polarization curves of the bare Mg, Mg samples with the *Mefp-1* film, the chitosan film and the CPC film after 7 d exposure in Hanks' solution.

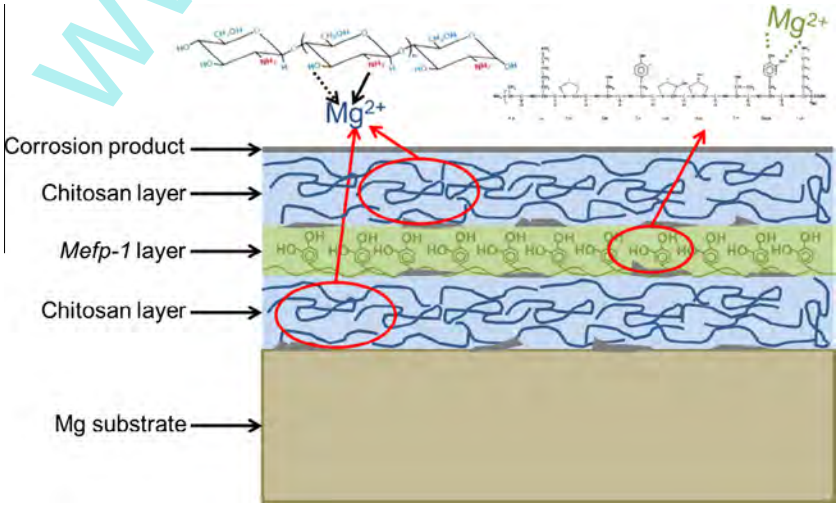

Fig. 7. Schematic illustration for the CPC film coated Mg immersed in Hanks' solution.

Table 2
The electrochemical parameters fitted from the potentiodynamic polarization curves.

Treatment	i_{corr} (μA cm^{-2})	E_{corr} (V_{SCE})	R_p (kΩ cm^2)	E_b (V_{SCE})
Mefp-1 film	15.5	−1.60	7.84	−1.32
Chitosan film	4.27	−1.53	12.39	−1.39
CPC film	1.93	−1.59	55.38	−1.25

Mefp-1 film and the chitosan film coated samples, and the R_p value was 4.5–7 times higher. Additionally, a more positive breakdown potential value indicated a much more compact and stronger-adhered film of CPC immobilized on the substrate. Combined with the EIS results, it can be concluded that the CPC film is able to significantly improve the corrosion resistance of the Mg substrate and control the degradation of Mg biomaterials.

3.4. Immersion tests

Fig. 9 shows the surface morphologies and element analysis of bare Mg and Mg coated with different films immersed in Hanks' solution for 7 d. The blow-up corrosion products layer on bare Mg substrate can be observed due to the evolution of hydrogen bubbles and formation of corrosion product $Mg(OH)_2$, and the occurrence of cracks on corrosion products was caused by the dehydration in the drying process [55,56]. On the chitosan and the CPC films, the cracks were deeper and severer, which could be ascribed to the higher thickness of the two films. Obviously, the more severe local damage was presented on the surfaces of the bare Mg and the *Mefp-1* film coated sample, and unevenly distributed corrosion products particles or aggregates were observed for the Mg modified by the chitosan film, indicating the non-uniform degradation of the substrates occurred in Hanks' solution. While the corrosion products on the CPC film surface distributed relatively uniformly, suggesting the homogenous chemical activity of Mg with the CPC film.

The EDX analysis showed that the corrosion products after immersion tests were composed of C, O, Mg, P, and Ca, except that P was absent on the bare Mg substrate (within the marked scope). The existence of Ca and P in the coated samples was considered to be beneficial to the biocompatibility. Compared with the CPC film, the higher contents of Ca and P for the chitosan film coated Mg substrate were attributed to the uneven distribution of corrosion products. Affected by the penetration depth of the electron beam

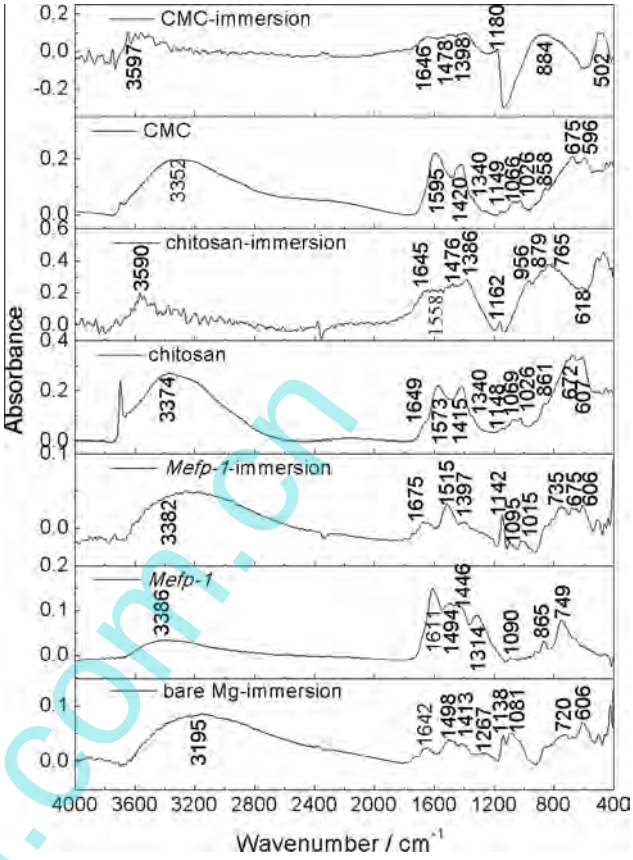

Fig. 10. IRAS spectra of Mg and Mg with the *Mefp-1* film, the chitosan film and the CPC film before and after immersion in Hanks' solution.

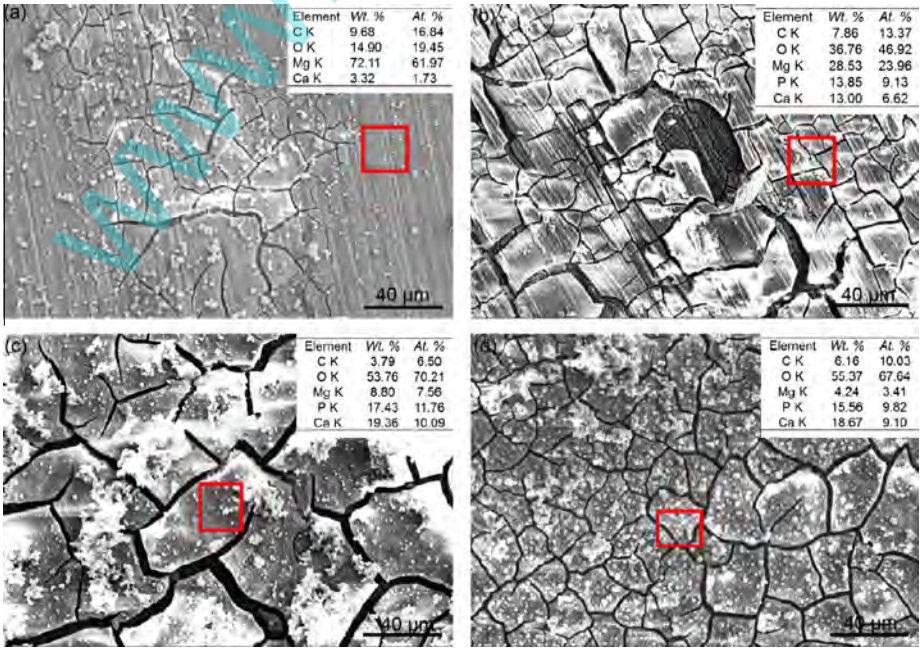

Fig. 9. Surface morphologies and EDX results for the sites marked by the red square of (a) Mg and Mg with (b) the *Mefp-1* film, (c) the chitosan film and (d) the CPC film after immersion in Hanks' solution for 7 d.

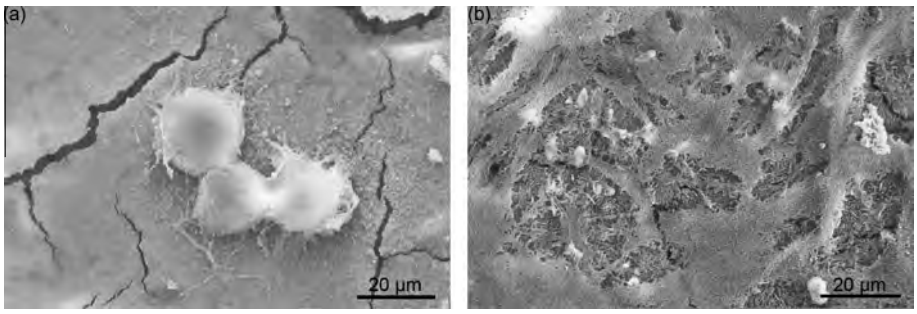

Fig. 11. SEM images of MC3T3-E1 cells on (a) Mg and (b) the CPC film coated Mg cultured for 4 d.

[57], the remarkable difference in the content of Mg for the *Mefp-1* film and CPC film could be ascribed to two reasons: the distinctively different thicknesses and corrosion protective properties of the films according to the cross-sectional SEM and EIS results. It is well known that the dissolution of Mg can be summarized as below [58]:

$$Mg(s) \rightarrow Mg^{2+}(aq) + 2e(\text{anodic reaction}) \quad (4)$$

$$2H_2O + 2e \rightarrow H_2(g) + 2OH^-(aq)(\text{cathodic reaction}) \quad (5)$$

$$Mg^{2+}(aq) + 2OH^-(aq) \rightarrow Mg(OH)_2(s) \quad (6)$$

where the $Mg(OH)_2$ was the primary corrosion product of Mg. While in simulated body fluid, there were also precipitated carbonates and phosphates, dihydrogen phosphate and hydrogen phosphate due to the local alkalization occurring on the Mg surface [43]. To clarify the compositions of corrosion products, the IRAS spectra of the bare Mg and the three coated samples were measured and compared with those before the immersion tests, as shown in Fig. 10. Obviously, the characteristic peaks of *Mefp-1*, chitosan and CPC films were replaced by those peaks centered at 1645 cm^{-1}, 1478 cm^{-1}, 1390 cm^{-1} and 1160 cm^{-1}, which were assigned to the OH^-, CO_3^{2-}, $H_2PO_4^-$ and PO_4^{3-} groups, respectively [59–61]. The results indicated that the corrosion products mainly contained phosphate, carbonate and hydroxide, which was in agreement with the EDX results.

3.5. Cell adhesion morphology

Fig. 11 shows the morphologies of MC3T3-E1 cells attached on the bare Mg and the CPC film coated Mg cultured for 4 d in the cell culture medium. The cells on bare Mg did not spread well and were in spherical shape, while those on the CPC film coated Mg exhibited obvious spreading appearance. The filopodia spread well and grew to be thin membranes as the cells adhered to the surface. The results implied that the surface of the bare Mg was not friendly to the cell because too fast corrosion rate of Mg induced a high alkalinity at the interface of cell/Mg substrate. In contrast, when corrosion of Mg was appropriately controlled by the CPC modification, the cultured cell attached and developed well on the coated Mg substrate, not only due to the excellent bio-properties of the CPC film, but also the biocompatible environment at the cell/CPC/Mg interface.

4. Conclusions

To control the biodegradation of medical Mg in body fluid environment, a protective and biocompatible composite film of chitosan/*Mefp-1*/chitosan (CPC) was successfully electrodeposited on Mg surface for the first time. The compact CPC film was able to play an effective barrier for Mg substrate to the surrounding environment. The ability of corrosion protection of the single film, either the *Mefp-1* film or the chitosan film, was low and only lasted for a short period. In comparison, the CPC composite film provided a much higher corrosion protection to Mg in a biophysical condition. In particular, the corrosion protection of the CPC film was even continually enhanced with the increase of immersion time in Hanks' solution to 7 d, which may be attributed to the synergistic reaction of *Mefp-1* and chitosan, and chelate effect with Mg^{2+} ion during the extended immersion time. Moreover, the CPC film facilitated the uniform degradation of Mg and inhibited the occurrence of local corrosion, which was beneficial to improve biocompatibility of the Mg medical devices based on the homogenous corrosion products film composed of phosphate, carbonate and hydroxide. The fact of the active attachment and spreading of MC3T3-E1 cells on the CPC film coated Mg substrate proved that the biocompatibility of the substrate was remarkably improved when the corrosion was appropriately controlled. To achieve the clinical application of the Mg-based medical devices, the future research will focus on the precisely controllable biodegradation of magnesium modified by the CPC film to fit the body rehabilitation of the patients.

Acknowledgments

This work was supported by International Science & Technology Cooperation Program of China (2014DFG52350) and National Natural Science Foundation of China (51571169).

References

[1] G.L. Song, Control of biodegradation of biocompatable magnesium alloys, Corros. Sci. 49 (2007) 1696–1701, http://dx.doi.org/10.1016/j.corsci.2007.01.001.
[2] S. Shadanbaz, G.J. Dias, Calcium phosphate coatings on magnesium alloys for biomedical applications: a review, Acta Biomater. 8 (2012) 20–30, http://dx.doi.org/10.1016/j.actbio.2011.10.016.
[3] N.T. Kirkland, J. Lespagnol, N. Birbilis, M.P. Staiger, A survey of bio-corrosion rates of magnesium alloys, Corros. Sci. 52 (2010) 287–291, http://dx.doi.org/10.1016/j.corsci.2009.09.033.
[4] M.P. Staiger, A.M. Pietak, J. Huadmai, G. Dias, Magnesium and its alloys as orthopedic biomaterials: a review, Biomaterials 27 (2006) 1728–1734, http://dx.doi.org/10.1016/j.biomaterials.2005.10.003.
[5] X.B. Chen, N. Birbilis, T.B. Abbott, A simple route towards a hydroxyapatite–Mg$(OH)_2$ conversion coating for magnesium, Corros. Sci. 53 (2011) 2263–2268, http://dx.doi.org/10.1016/j.corsci.2011.03.008.
[6] F. Witte, J. Fischer, J. Nellesen, C. Vogt, J. Vogt, T. Donath, F. Beckmann, In vivo corrosion and corrosion protection of magnesium alloy LAE442, Acta Biomater. 6 (2010) 1792–1799, http://dx.doi.org/10.1016/j.actbio.2009.10.012.
[7] H. Hornberger, S. Virtanen, A. Boccaccini, Biomedical coatings on magnesium alloys–a review, Acta Biomater. 8 (2012) 2442–2455, http://dx.doi.org/10.1016/j.actbio.2012.04.012.
[8] E. Zhang, L. Yang, Microstructure, mechanical properties and bio-corrosion properties of Mg–Zn–Mn–Ca alloy for biomedical application, Mater. Sci. Eng., A 497 (2008) 111–118, http://dx.doi.org/10.1016/j.msea.2008.06.019.
[9] C. op't Hoog, N. Birbilis, Y. Estrin, Corrosion of pure Mg as a function of grain size and processing route, Adv. Eng. Mater. 10 (2008) 579–582, http://dx.doi.org/10.1002/adem.200800046.
[10] S. Virtanen, Biodegradable Mg and Mg alloys: corrosion and biocompatibility, Mater. Sci. Eng., B 176 (2011) 1600–1608, http://dx.doi.org/10.1016/j.mseb.2011.05.028.

[11] A. Doraiswamy, R. Narayan, R. Cristescu, I. Mihailescu, D. Chrisey, Laser processing of natural mussel adhesive protein thin films, Mater. Sci. Eng., C 27 (2007) 409–413, http://dx.doi.org/10.1016/j.msec.2006.05.026.
[12] T.J. Deming, Mussel byssus and biomolecular materials, Curr. Opin. Chem. Biol. 3 (1999) 100–105, http://dx.doi.org/10.1016/S1367-5931(99)80018-0.
[13] M. Rinaudo, Chitin and chitosan: properties and applications, Prog. Polym. Sci. 31 (2006) 603–632, http://dx.doi.org/10.1016/j.progpolymsci.2006.06.001.
[14] J. Carneiro, J. Tedim, M. Ferreira, Chitosan as a smart coating for corrosion protection of aluminum alloy 2024: a review, Prog. Org. Coat. 89 (2015) 348–356, http://dx.doi.org/10.1016/j.porgcoat.2015.03.008.
[15] F. Zhang, J. Pan, P.M. Claesson, Electrochemical and AFM studies of mussel adhesive protein (*Mefp-1*) as corrosion inhibitor for carbon steel, Electrochim. Acta 56 (2011) 1636–1645, http://dx.doi.org/10.1016/j.electacta.2010.10.033.
[16] X. Gu, Y. Zheng, Q. Lan, Y. Cheng, Z. Zhang, T. Xi, D. Zhang, Surface modification of an Mg-1Ca alloy to slow down its biocorrosion by chitosan, Biomed. Mater. 4 (2009) 044109, http://dx.doi.org/10.1088/1748-6041/4/4/044109.
[17] J.H. Waite, Nature's underwater adhesive specialist, Int. J. Adhes. Adhes. 7 (1987) 9–14, http://dx.doi.org/10.1016/0143-7496(87)90048-0.
[18] C. Sun, J.H. Waite, Mapping chemical gradients within and along a fibrous structural tissue, mussel byssal threads, J. Biol. Chem. 280 (2005) 39332–39336, http://dx.doi.org/10.1074/jbc.M508674200.
[19] M.J. Harrington, A. Masic, N. Holten-Andersen, J.H. Waite, P. Fratzl, Iron-clad fibers: a metal-based biological strategy for hard flexible coatings, Science 328 (2010) 216–220, http://dx.doi.org/10.1126/science.1181044.
[20] M. Yu, J. Hwang, T.J. Deming, Role of L-3, 4-dihydroxyphenylalanine in mussel adhesive proteins, J. Am. Chem. Soc. 121 (1999) 5825–5826.
[21] Q. Lu, E. Danner, J.H. Waite, J.N. Israelachvili, H. Zeng, D.S. Hwang, Adhesion of mussel foot proteins to different substrate surfaces, J. Roy. Soc. Interf. 10 (2013) 20120759, http://dx.doi.org/10.1098/rsif.2012.0759.
[22] T.H. Anderson, J. Yu, A. Estrada, M.U. Hammer, J.H. Waite, J.N. Israelachvili, The contribution of DOPA to substrate-peptide adhesion and internal cohesion of mussel-inspired synthetic peptide films, Adv. Funct. Mater. 20 (2010) 4196–4205, http://dx.doi.org/10.1002/adfm.201000932.
[23] H. Lee, N.F. Scherer, P.B. Messersmith, Single-molecule mechanics of mussel adhesion, Proc. Natl. Acad. Sci. 103 (2006) 12999–13003, http://dx.doi.org/10.1073/pnas.0605552103.
[24] F. Zhang, J. Pan, P.M. Claesson, T. Brinck, Electrochemical, atomic force microscopy and infrared reflection absorption spectroscopy studies of pre-formed mussel adhesive protein films on carbon steel for corrosion protection, Thin Solid Films 520 (2012) 7136–7143, http://dx.doi.org/10.1016/j.tsf.2012.07.115.
[25] F. Zhang, M. Sababi, T. Brinck, D. Persson, J. Pan, P.M. Claesson, *In situ* investigations of Fe^{3+} induced complexation of adsorbed *Mefp-1* protein film on iron substrate, J. Colloid Interf. Sci. 404 (2013) 62–71, http://dx.doi.org/10.1016/j.jcis.2013.05.016.
[26] U. Grienke, J. Silke, D. Tasdemir, Bioactive compounds from marine mussels and their effects on human health, Food Chem. 142 (2014) 48–60, http://dx.doi.org/10.1016/j.foodchem.2013.07.027.
[27] M.N. Ravi Kumar, A review of chitin and chitosan applications, React. Funct. Polym. 46 (2000) 1–27, http://dx.doi.org/10.1016/S1381-5148(00)00038-9.
[28] H. Yi, L.Q. Wu, W.E. Bentley, R. Ghodssi, G.W. Rubloff, J.N. Culver, G.F. Payne, Biofabrication with chitosan, Biomacromolecules 6 (2005) 2881–2894, http://dx.doi.org/10.1021/bm050410l.
[29] M. Zheludkevich, J. Tedim, C. Freire, S. Fernandes, S. Kallip, A. Lisenkov, A. Gandini, M. Ferreira, Self-healing protective coatings with "green" chitosan based pre-layer reservoir of corrosion inhibitor, J. Mater. Chem. 21 (2011) 4805–4812, http://dx.doi.org/10.1039/c1jm10304k.
[30] K.F. Bai, Y. Zhang, Z.Y. Fu, C.L. Zhang, X.Z. Cui, E.C. Meng, S.K. Guan, J.H. Hu, Fabrication of chitosan/magnesium phosphate composite coating and the in vitro degradation properties of coated magnesium alloy, Mater. Lett. 73 (2012) 59–61, http://dx.doi.org/10.1016/j.matlet.2011.12.102.
[31] P. Liu, X. Pan, W.H. Yang, K.Y. Cai, Y.S. Chen, Improved anticorrosion of magnesium alloy via layer-by-layer self-assembly technique combined with micro-arc oxidation, Mater. Lett. 75 (2012) 118–121, http://dx.doi.org/10.1016/j.matlet.2012.02.016.
[32] C.L. Ouyang, T. Lei, L. Wang, N.F. Li, L.S. Zhou, Corrosion behaviours of ternary Mg-Zn-Ca alloy biomaterials, Chin. J. Nonferr. Met. 20 (2010) 891–897.
[33] Y. Li, X. Pang, R. Epand, I. Zhitomirsky, Electrodeposition of chitosan-hemoglobin films, Mater. Lett. 65 (2011) 1463–1465, http://dx.doi.org/10.1016/j.matlet.2011.02.038.
[34] L. Lim, L.S. Wan, Heat treatment of chitosan films, Drug Dev. Ind. Pharm. 21 (1995) 839–846, http://dx.doi.org/10.3109/03639049509026648.
[35] G.C. Ritthidej, T. Phaechamud, T. Koizumi, Moist heat treatment on physicochemical change of chitosan salt films, Int. J. Pharm. 232 (2002) 11–22, http://dx.doi.org/10.1016/S0378-5173(01)00894-8.
[36] V.V. Papov, T.V. Diamond, K. Biemann, J.H. Waite, Hydroxyarginine-containing polyphenolic proteins in the adhesive plaques of the marine mussel *Mytilus edulis*, J. Biol. Chem. 270 (1995) 20183–20192, http://dx.doi.org/10.1074/jbc.270.34.20183.
[37] H. Ceylan, M. Urel, T.S. Erkal, A.B. Tekinay, A. Dana, M.O. Guler, Mussel inspired dynamic cross-linking of self-healing peptide nanofiber network, Adv. Funct. Mater. 23 (2013) 2081–2090, http://dx.doi.org/10.1002/adfm.201202291.
[38] C.Q. Ye, R.G. Hu, S.G. Dong, X.J. Zhang, R.Q. Hou, R.G. Du, C.J. Lin, J.S. Pan, EIS analysis on chloride-induced corrosion behavior of reinforcement steel in simulated carbonated concrete pore solutions, J. Electroanal. Chem. 688 (2013) 275–281, http://dx.doi.org/10.1016/j.jelechem.2012.09.012.
[39] I. Amaral, M. Lamghari, S. Sousa, P. Sampaio, M. Barbosa, Rat bone marrow stromal cell osteogenic differentiation and fibronectin adsorption on chitosan membranes: the effect of the degree of acetylation, J. Biomed. Mater. Res. A 75 (2005) 387–397, http://dx.doi.org/10.1002/jbm.a.30436.
[40] J. Wang, J. Tang, P. Zhang, Y. Li, J. Wang, Y. Lai, L. Qin, Surface modification of magnesium alloys developed for bioabsorbable orthopedic implants: a general review, J. Biomed. Mater. Res. B Appl. Biomater. 100 (2012) 1691–1701, http://dx.doi.org/10.1002/jbm.b.32707.
[41] K. Yamada, T. Chen, G. Kumar, O. Vesnovsky, L.T. Topoleski, G.F. Payne, Chitosan based water-resistant adhesive. Analogy to mussel glue, Biomacromolecules 1 (2000) 252–258, http://dx.doi.org/10.1021/bm0003009.
[42] S. Keera, M. Deyab, Effect of some organic surfactants on the electrochemical behaviour of carbon steel in formation water, Colloids Surf. A 266 (2005) 129–140, http://dx.doi.org/10.1016/j.colsurfa.2005.05.069.
[43] Z. Li, G.L. Song, S. Song, Effect of bicarbonate on biodegradation behaviour of pure magnesium in a simulated body fluid, Electrochim. Acta 115 (2014) 56–65, http://dx.doi.org/10.1016/j.electacta.2013.10.131.
[44] C. Liu, Y. Xin, X. Tian, P.K. Chu, Degradation susceptibility of surgical magnesium alloy in artificial biological fluid containing albumin, J. Mater. Res. 22 (2007) 1806–1814, http://dx.doi.org/10.1557/jmr.2007.0241.
[45] Y. Xin, K. Huo, H. Tao, G. Tang, P.K. Chu, Influence of aggressive ions on the degradation behavior of biomedical magnesium alloy in physiological environment, Acta Biomater. 4 (2008) 2008–2015, http://dx.doi.org/10.1016/j.actbio.2008.05.014.
[46] X. Gu, Y. Zheng, L. Chen, Influence of artificial biological fluid composition on the biocorrosion of potential orthopedic Mg–Ca, AZ31, AZ91 alloys, Biomed. Mater. 4 (2009) 065011, http://dx.doi.org/10.1088/1748-6041/4/6/065011.
[47] J.M. McIntyre, H.Q. Pham, Electrochemical impedance spectroscopy; a tool for organic coatings optimizations, Prog. Org. Coat. 27 (1996) 201–207, http://dx.doi.org/10.1016/0300-9440(95)00532-3.
[48] N.C. Rosero-Navarro, S. Pellice, A. Durán, M. Aparicio, Effects of Ce-containing sol–gel coatings reinforced with SiO_2 nanoparticles on the protection of AA2024, Corros. Sci. 50 (2008) 1283–1291, http://dx.doi.org/10.1016/j.corsci.2008.01.031.
[49] Y. Gu, S. Bandopadhyay, C. Chen, Y. Guo, C. Ning, Effect of oxidation time on the corrosion behavior of micro-arc oxidation produced AZ31 magnesium alloys in simulated body fluid, J. Alloys Compd. 543 (2012) 109–117, http://dx.doi.org/10.1016/j.jallcom.2012.07.130.
[50] X. Zhong, Q. Li, J. Hu, Y. Lu, Characterization and corrosion studies of ceria thin film based on fluorinated AZ91D magnesium alloy, Corros. Sci. 50 (2008) 2304–2309, http://dx.doi.org/10.1016/j.corsci.2008.05.016.
[51] G. Liu, S. Tang, D. Li, J. Hu, Self-adjustment of calcium phosphate coating on micro-arc oxidized magnesium and its influence on the corrosion behaviour in simulated body fluids, Corros. Sci. 79 (2014) 206–214, http://dx.doi.org/10.1016/j.corsci.2013.11.011.
[52] A. Witecka, A. Yamamoto, J. Idaszek, A. Chlanda, W. Święszkowski, Influence of biodegradable polymer coatings on corrosion, cytocompatibility and cell functionality of Mg-2.0Zn-0.98Mn magnesium alloy, Colloids Surf. B 144 (2016) 284–292, http://dx.doi.org/10.1016/j.colsurfb.2016.04.021.
[53] B.P. Frank, G. Belfort, Adhesion of *Mytilus edulis* foot protein 1 on silica: ionic effects on biofouling, Biotechnol. Progr. 18 (2002) 580–586, http://dx.doi.org/10.1021/bp010140s.
[54] X.M. Yang, M. Li, X. Lin, L.L. Tan, G.B. Lan, L.H. Li, Q.S. Yin, H. Xia, Y. Zhang, K. Yang, Enhanced in vitro biocompatibility/bioactivity of biodegradable Mg-Zn-Zr alloy by micro-arc oxidation coating contained Mg_2SiO_4, Surf. Coat. Technol. 233 (2013) 65–73, http://dx.doi.org/10.1016/j.surfcoat.2013.01.052.
[55] G. Wu, X. Zeng, G. Yuan, Growth and corrosion of aluminum PVD-coating on AZ31 magnesium alloy, Mater. Lett. 62 (2008) 4325–4327, http://dx.doi.org/10.1016/j.matlet.2008.07.014.
[56] Y. Song, D. Shan, R. Chen, F. Zhang, E.-H. Han, Biodegradable behaviors of AZ31 magnesium alloy in simulated body fluid, Mater. Sci. Eng., C 29 (2009) 1039–1045, http://dx.doi.org/10.1016/j.msec.2008.08.026.
[57] C. Lorenz, J.G. Brunner, P. Kollmannsberger, L. Jaafar, B. Fabry, S. Virtanen, Effect of surface pre-treatments on biocompatibility of magnesium, Acta Biomater. 5 (2009) 2783–2789, http://dx.doi.org/10.1016/j.actbio.2009.04.018.
[58] Z. Li, X. Gu, S. Lou, Y. Zheng, The development of binary Mg-Ca alloys for use as biodegradable materials within bone, Biomaterials 29 (2008) 1329–1344, http://dx.doi.org/10.1016/j.biomaterials.2007.12.021.
[59] D.X. Liu, K. Savino, M.Z. Yates, Coating of hydroxyapatite films on metal substrates by seeded hydrothermal deposition, Surf. Coat. Technol. 205 (2011) 3975–3986, http://dx.doi.org/10.1016/j.surfcoat.2011.02.008.
[60] C. Wen, S. Guan, L. Peng, C. Ren, X. Wang, Z. Hu, Characterization and degradation behavior of AZ31 alloy surface modified by bone-like hydroxyapatite for implant applications, Appl. Surf. Sci. 255 (2009) 6433–6438, http://dx.doi.org/10.1016/j.apsusc.2008.09.078.
[61] J.E. Gray-Munro, C. Seguin, M. Strong, Influence of surface modification on the in vitro corrosion rate of magnesium alloy AZ31, J. Biomed. Mater. Res., A 91 (2009) 221–230, http://dx.doi.org/10.1002/jbm.a.32205.